

Supplementary Information

One Dimensional Building Block for Molecular Separation: Laminated Graphitic Nanoribbons

Dae Woo Kim^{a}, In Kim^b, Jidon Jang^b, Yoon Tae Nam^a, Kangho Park^a, Ki Ok Kwon^a, Kyoung Min Cho^a, Junghoon Choi^a, Daeok Kim^b, Kyoung Min Kang^a, Seon Joon Kim^a, Yousung Jung^b and Hee-Tae Jung^{a*}*

^a National Laboratory for Organic Opto-Electronic Materials, Department of Chemical and Biomolecular Eng. (BK-21 plus) & KAIST Institute for Nanocentury, Korea Advanced Institute of Science and Technology, Daejeon 305-701, Republic of Korea

^b Graduate School of Energy, Environment, Water, and Sustainability (EEWS), Korea Advanced Institute of Science and Technology, Daejeon 305-701, Republic of Korea

*Corresponding authors. E-mail: audw1105@kaist.ac.kr (D.W. Kim) & heetae@kaist.ac.kr (H.-T. Jung).

Materials and methods

Preparation of GONR: Multiwall carbon nanotubes (MWCNTs) were purchased from Hanwha Chemical (CM-150). MWCNTs (100 mg) and KMnO_4 (500 mg) were mixed in a 100 mL H_2SO_4 solution. The mixture was stirred at 35 °C for 15 h, and then 200 mL of deionized (DI) water was added slowly to the mixture in an ice bath. Hydrogen peroxide (10 mL) was also added. To remove the reacted acidic solution, the mixtures were subjected to centrifugation at 15000 rpm for 1 h at 4 °C, and the supernatants were removed. The remaining GONRs were redispersed in water and subjected to centrifugation at 5000 rpm for 1 h at 4 °C to remove the bundled CNTs or thick GONRs. Supernatants were collected and used to fabricate the GONR membranes. As previously reported [1], unzipping is initiated by the formation of manganite esters through the sp^2 carbons in the CNT wall. By the reaction with a strong oxidizing agent (e.g., KMnO_4), ketone groups on the surface of CNTs were retained. Once the functional groups were generated, the density of the ketone groups increased, and then the CNTs were longitudinally unzipped to reduce the strain in the nanotubes induced by the oxygen functional groups. The ketones at the GONR edge could be converted into carboxylic groups through O-protonated forms.

Preparation of rGONR: NaOH (100 mg) was mixed with the as-prepared GONR 100 mL solution. The mixture was annealed at 120 °C for 1 h by autoclaving. To remove the reacted NaOH, solutions were subjected to centrifugation at 15000 rpm for 1 h at 4 °C, and the supernatants were removed. The remaining rGONRs were redispersed in water and subjected to centrifugation at 5000 rpm for 1 h at 4 °C to remove the bundled rGONRs.

Supernatants were collected and used to fabricate the rGONR membranes.

Preparation of GO: GO was synthesized *via* the modified Hummer's method. Graphite powder (2 g) was added to a sulfuric acid solution (98%), and KMnO_4 (7 g) was slowly added to the mixture. The mixture was reacted at 35 °C for 2 h in a water bath, and then 200 mL of DI water was slowly added to the mixture in an ice bath. Hydrogen peroxide (10 mL) was also added. The solution of synthesized GO was passed through a paper filter and repeatedly washed with a hydrochloric acid solution (10%) to remove the remaining manganese impurities. After GO powder was obtained, GO was dispersed in DI water to a concentration of 0.1 mg/mL.

Fabrication of the membranes. Commercial track-etched PC filter (Whatman, 200 nm pore size), nylon (Whatman, 200 nm pore size), and AAO (Whatman, 200 nm pore size) were used as supporting substrates. The prepared GONR and rGONR solutions were diluted to a concentration of 0.001 mg/mL and then filtered under vacuum using a commercial filter. The thicknesses of GNR and rGONR membranes were determined by controlling the amounts of dispersion filtered. The membrane was dried in a 70 °C oven for 30 min to remove the remaining water in the membrane films.

Evaluation of membrane performance: The filtration performance of the membrane was evaluated using the dyes MR, MnB, RosB, and BB, as well as various salts. The effective area of the membrane under the operating pressure was 4.523 cm². All experiments were performed at room temperature (25 °C) using a dead-end filtration equipment built in-house, and the pressure was controlled by varying the pressure of nitrogen gas. Because a dead-end filtration system was used, the permeance and rejection of filtered solutions was typically obtained by analyzing 10 mL of the permeated solution to avoid the concentration polarization of molecules on the membrane surface during extended filtration. Permeance was calculated as follows,

$$\text{Permeance (L m}^{-2} \text{ h}^{-1} \text{ bar}^{-1}) = \frac{V_p}{t A \Delta P}$$

where V_p is the volume of the permeate solution, t is the permeation time, A is the effective area of the membrane, and ΔP is the nitrogen pressure.

$$\text{Rejection (\%)} = \frac{C_f - C_p}{C_f} \times 100(\%)$$

The rejection rates for the dye molecules were calculated by measuring the absorbance of the relevant peaks on an ultraviolet–visible spectrophotometer (Jasco V-570 UV/VIS/NIR). Calculations were based on Beer–Lambert law. The concentration of salt ions was measured using an ion conductivity meter.

Characterization: SEM images of the membranes were recorded on a field-emission scanning electron microscopy system (Nova 230). XPS spectra were obtained on a Thermo-VG Sigma probe, and AFM images were recorded on a Bruker Multimode 8 instrument with a Nanoscope V control station in the tapping mode. Raman spectra of CNTs, GO, GONR, and rGONR were recorded by dispersive Raman spectroscopy (Aramis, Horiba Jobin Yvon) with laser excitation at 514 nm. XRD patterns were recorded on a multipurpose thin-film X-

ray diffractometer (Rigaku).

Calculation of water flux of GNR via the classical Hagen–Poiseuille equation for slit-shaped pores: The

formula $Flux \approx \frac{h^4 \Delta P}{12L^2 \mu \Delta x}$ was used, where h is the interlayer spacing of the GNR film (~ 1 nm), L is the average lateral length of the GNR sheets (~ 20 nm), μ is the viscosity of water (0.001 Pa s at 20 °C), and Δx is the thickness of the GNR membrane [2].

Computational details: Binding energy was calculated using the Vienna *ab initio* simulation package [3] with the revised Perdew–Burke–Ernzerhof [4] and Grimme’s D3 dispersion correction [5]. A plane wave basis set and the projector-augmented wave method with a cutoff energy of 500 eV were used. Geometries were fully optimized until the force was less than 0.05 eV Å⁻¹. All energies were sampled at gamma point. The periodic box boundary of the system is approximately $x = 17.04$ Å, $y = 17.22$ Å, and $z = 25$ Å.

For the MD simulations, two sets of models were used. A reservoir model was used to calculate the equilibrated density of toluene molecules in 2D confinement (both pristine and GO channels), and an infinite-plate model using the equilibrium density thus obtained was used for non-equilibrated MD simulations to study the toluene flow (**Fig. S25**). The mean absolute displacement of toluene molecules as a function of layer distance and surface oxidation states were analyzed. Hydroxyl groups were randomly attached to the interlayer channel surfaces with a density defined as a ratio of the number of hydroxyl-attached carbons to the total number of carbons on graphene. All MD simulations were performed using the LAMMPS package [6] with a quantum-mechanics-based force field (QMFF-Cx) [7] for graphitic carbons. DREIDING force field [8] was used for the hydroxyl groups, similar to a method reported elsewhere [9]. The OPLS-AA force field [10] was used for toluene molecules.

The MD simulations in this study were composed of four steps. First, the system was minimized by steepest-descent and conjugate-gradient algorithms in the reservoir system. Second, the system was heated to room temperature (298 K) over 0.2 ns in the NVT ensemble with a Nosé–Hoover thermostat. After initial equilibration, a 2 ns equilibrium simulation of NPT dynamics at a constant pressure (1 atm) and constant temperature was performed. This yielded an equilibrium density of toluene molecules inside the two-dimensional confined space. Finally, non-equilibrium simulations were performed in the infinite-plate configuration with a toluene density obtained from the equilibrium simulations described above. In this system, 0.1 kcal/mol Å of force was applied to all of the toluene molecules in the channel to allow the net flow of toluene molecules in the NVT ensemble.

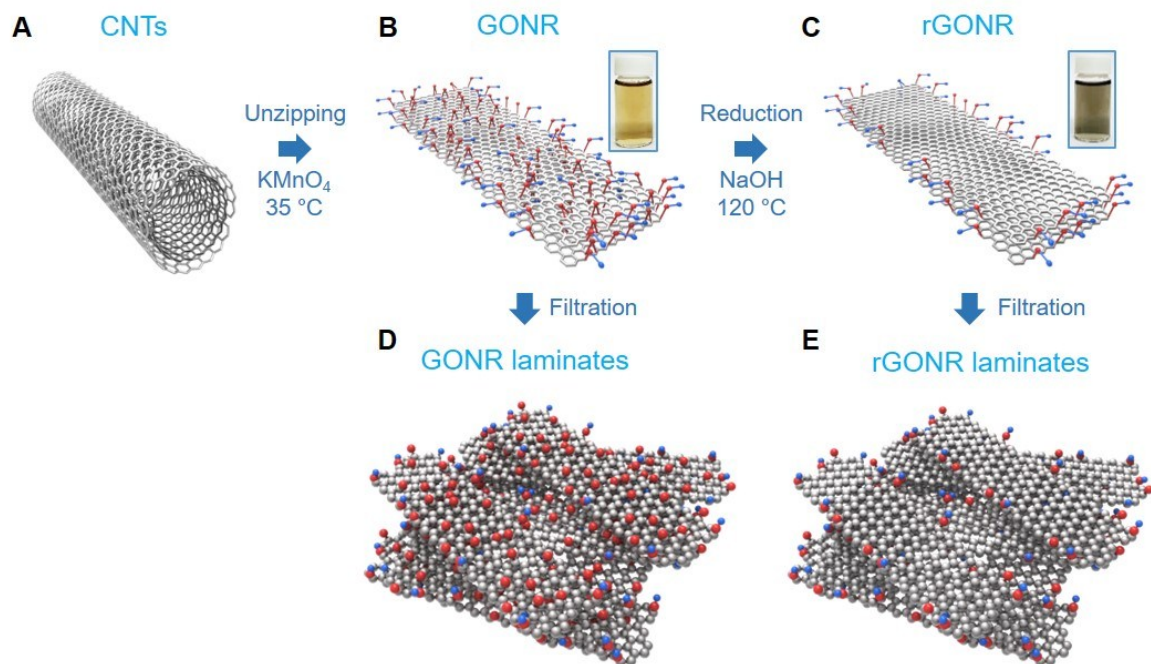


Fig. S1 Preparation of graphene nanoribbon laminated membranes. (A) MWCNTs. (B) GONRs prepared by chemical unzipping using a KMnO_4 solution. (C) Reduced graphene nanoribbons upon NaOH treatment. Insets in (B) and (C) are photographs of GONR and rGONR dispersions (0.01 mg/mL). (D) and (E) Schematic of the graphene nanoribbon laminated membranes prepared by the filtration of graphene nanoribbon dispersions.

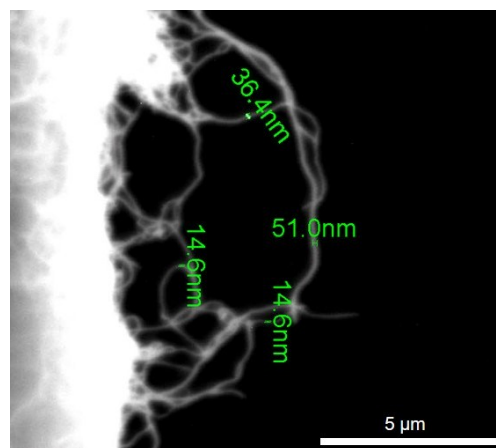


Fig. S2 SEM image of multiwall CNTs.

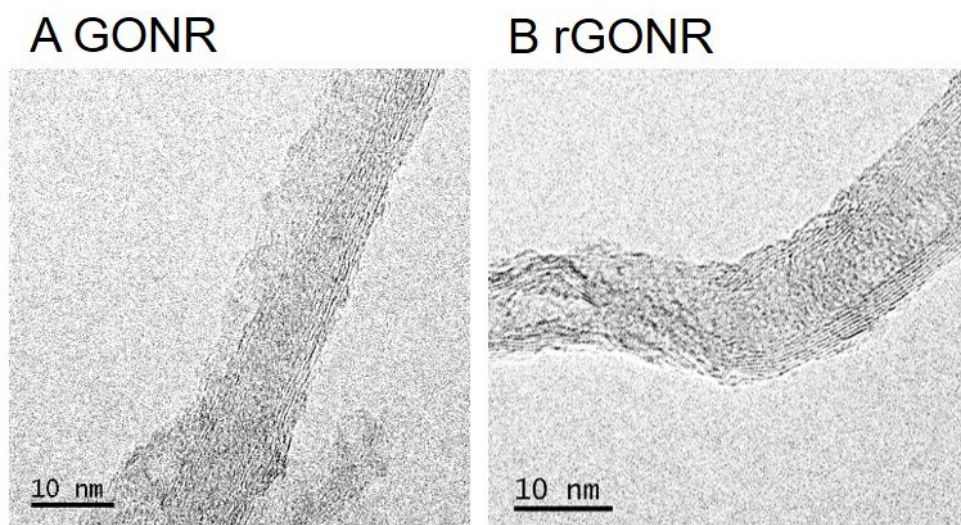


Fig. S3 TEM images of (A) GONR and (B) rGONR.

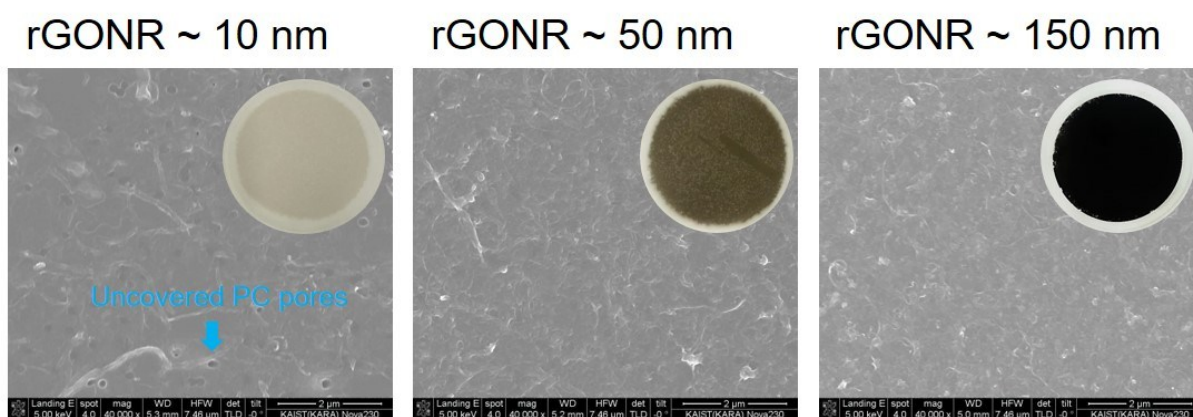


Fig. S4 Photographs of the rGONR membranes of varying thicknesses and corresponding SEM images. When the rGONR or GONR films were very thin (<10 nm), open pores were observed on the polymer supports. The thickness of each membrane was measured by AFM. The filtration membranes were transferred from the AAO filter to the SiO₂ substrate by etching the AAO with a 3 M NaOH solution. Membranes floating on the water were scooped with the substrate and then dried in the oven at 70 °C for 1 h.

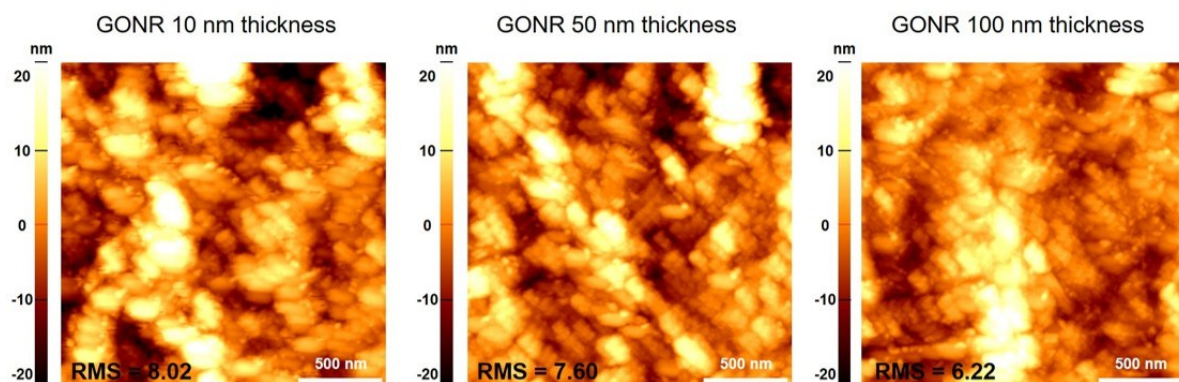


Fig. S5 AFM images obtained from the surface of GONR membranes depending on the thickness. GONR membrane showed the RMS value from 6 Å to 8 Å, indicating the smooth surface of the membrane.

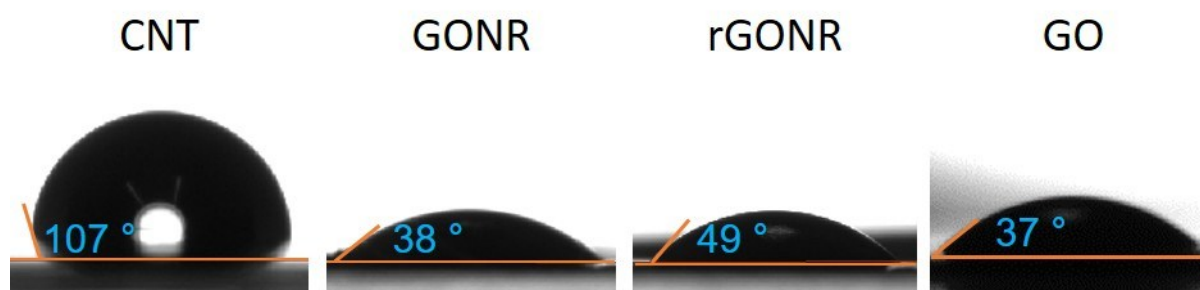
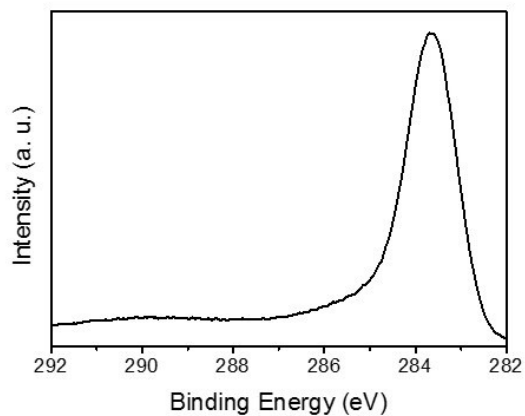
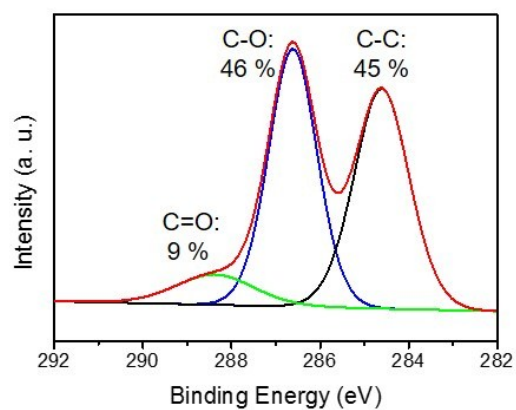


Fig. S6 Water contact angles on CNT, GONR, rGONR, and GO films. Here, the stronger hydrophilic properties of the GONR and rGONR membranes as compared with that of the CNT film are apparent.

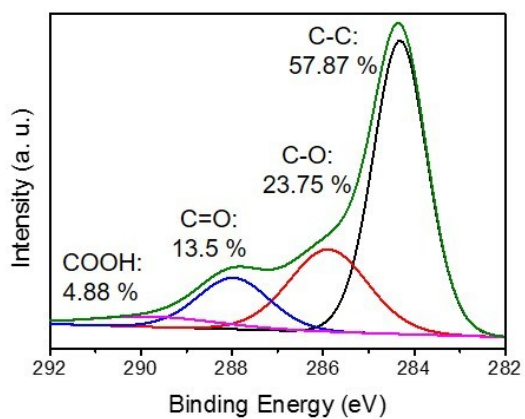
A CNT



B GO



C GONR



D rGONR

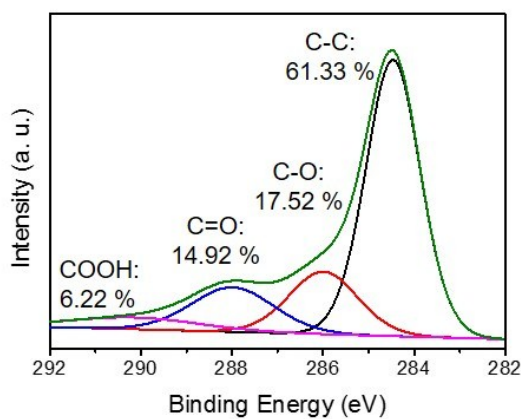


Fig. S7 XPS C1s spectra of **(A)** CNT, **(B)** GO, **(C)** GONR, and **(D)** rGONR.

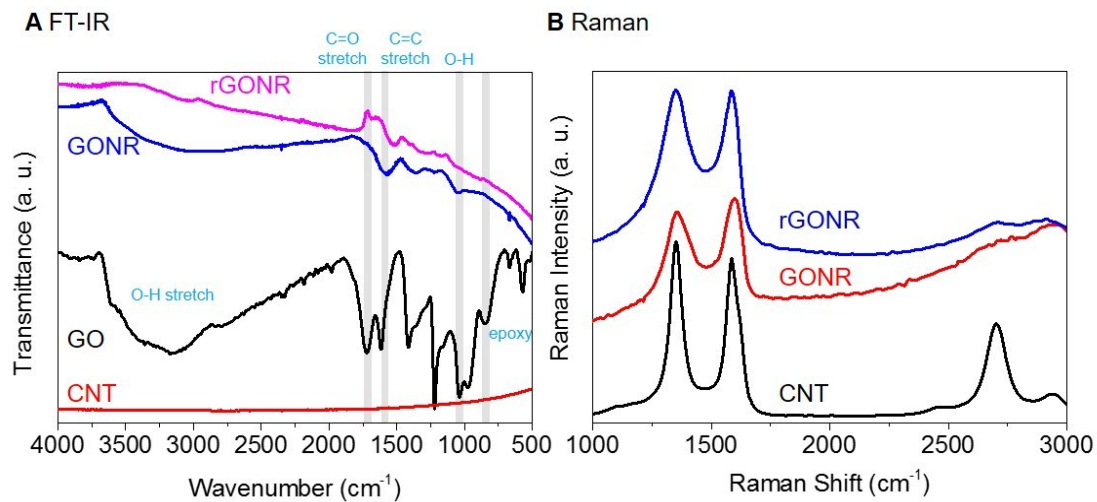


Fig. S8 (A) FTIR and **(B)** Raman spectra of CNT, GO, GONR, and rGONR.

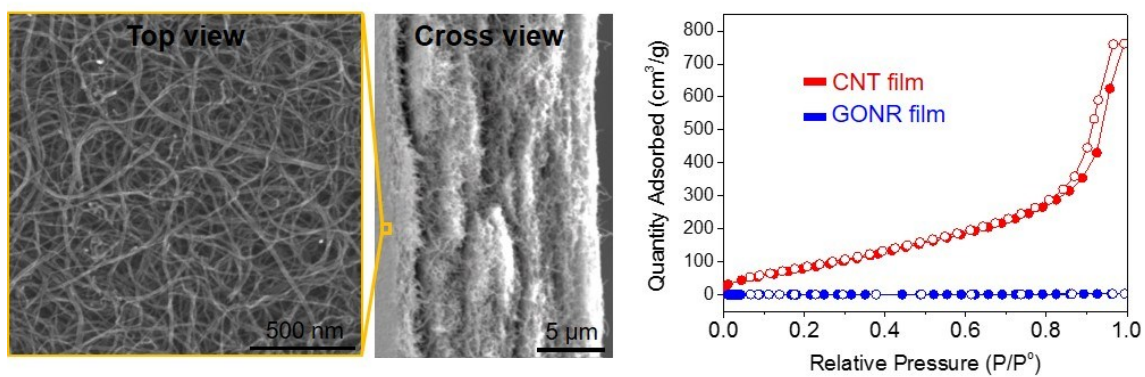


Fig. S9 SEM images of the CNT film and Ar isotherms for the CNT and GONR films.

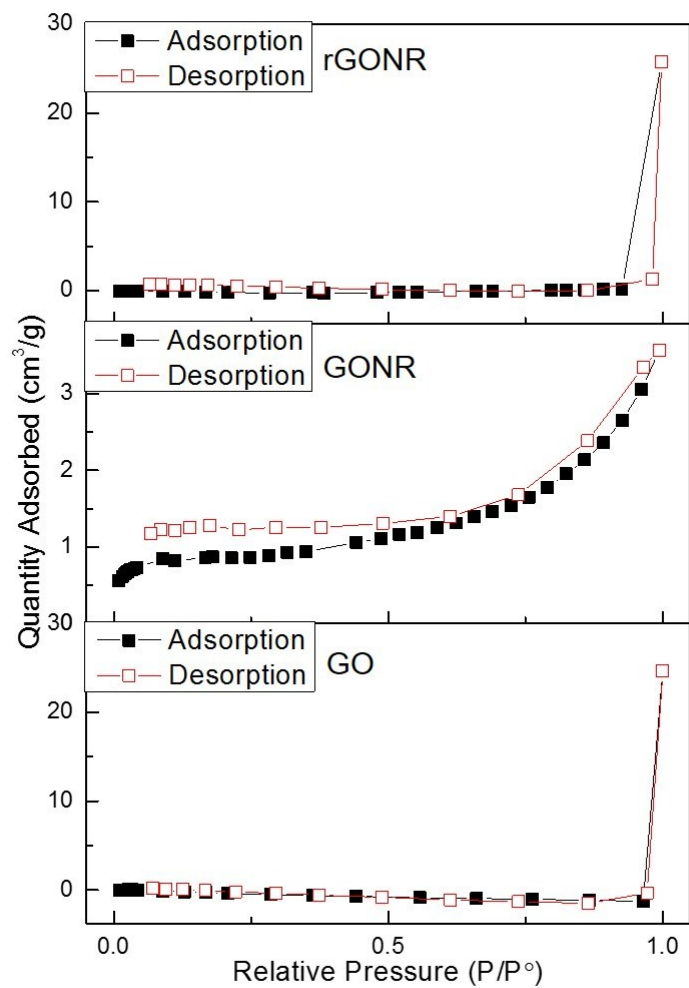


Fig. S10 Ar isotherms of GO, GONR, and rGONR films. The three samples showed a negligible amount of Ar adsorbed during argon isotherm measurement at 77 K, indicating nonporous characteristics of the materials related to the compact stacking of aromatic sheets.

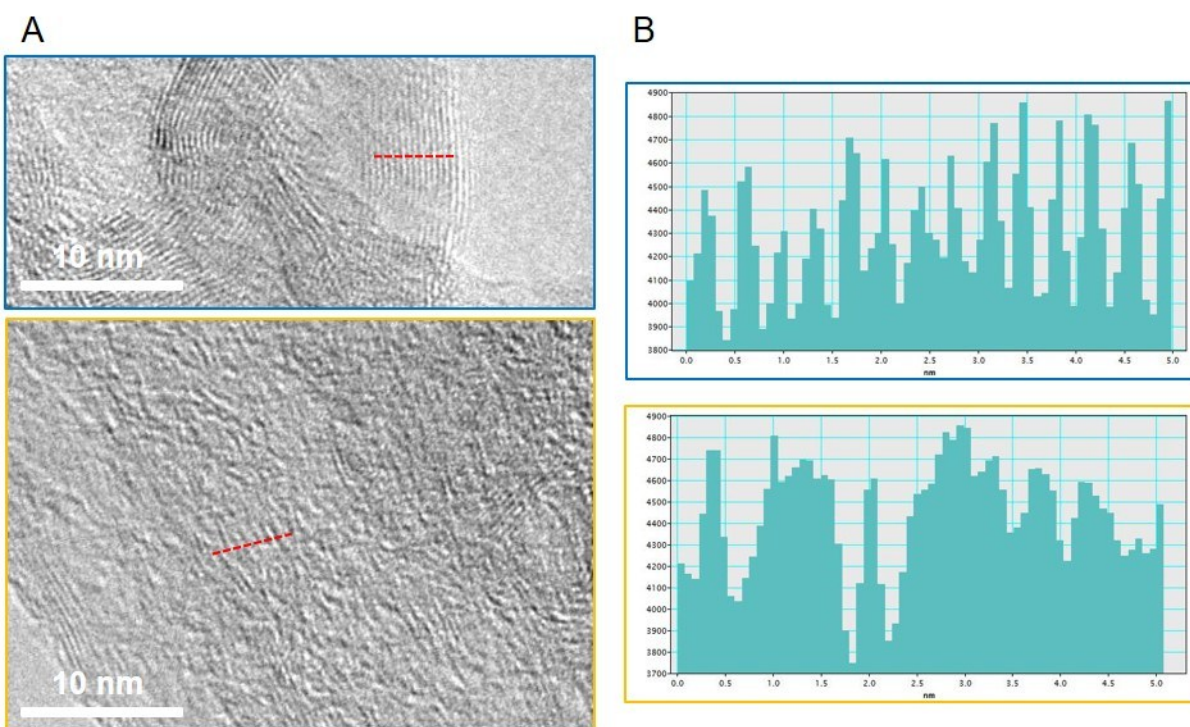


Fig. S11 (A) TEM images of the rGONR film. **(B)** Intensity profiles obtained from the stacked regions in the rGONR film marked in **(A)**. Typical interlayer spacing of the rGONR film at approximately 4 Å; larger spacing (up to approximately 8 Å) was occasionally observed.

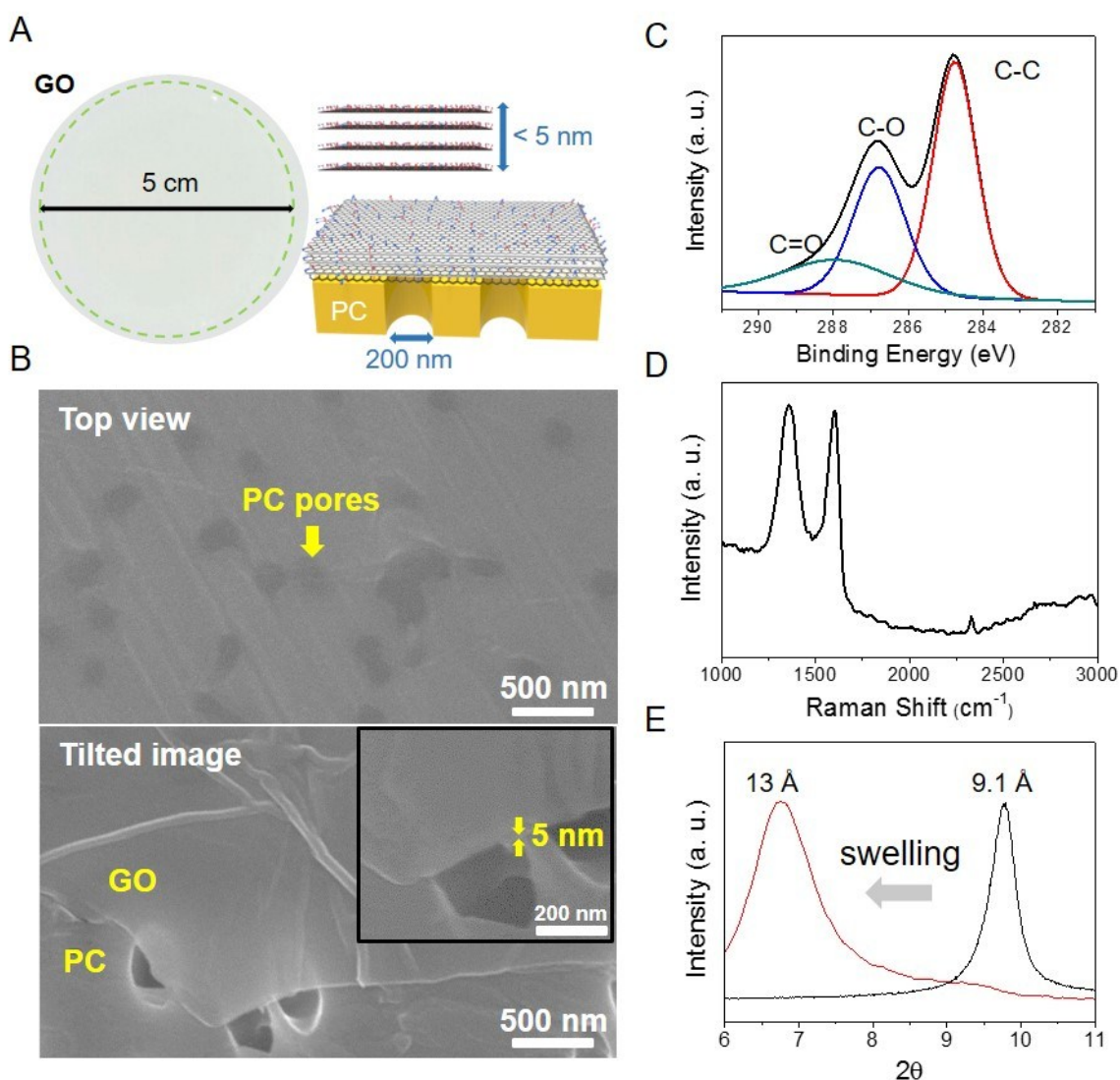


Fig. S12 (A) Photograph of a ~ 5 nm thick GO membrane on a PC filter and corresponding schematics. (B) SEM images of the top and tilted views of the GO membrane on the PC filter. (C) XPS C1s spectrum of the GO membrane. (D) Raman spectra of the GO membrane under a 514 nm beam. (E) XRD spectra obtained for the GO membrane before and after swelling in water.

The XPS C1s peak in **Fig. 12C** showed the evolution of peaks at 284.7, 286.7, and 288 eV, which respectively correspond to the C–C, C–O, and C=O bonds of oxidized graphene. The Raman spectrum obtained under 514 nm laser excitation also showed the highly defective structure of graphene upon the oxidation using the Hummer’s method, as well as the D-band peak at 1360 cm^{-1} and the G-band peak at 1606 cm^{-1} (**Fig. S12D**). XRD measurements were also conducted on both GO and GO films after immersion in the water (**Fig. 12E**). Because the multilayer film was too thin (5 nm thickness) to be investigated with conventional XRD equipment, a 200 nm thick GO film was prepared instead of 5 nm thick GO film. The film was immersed in water for 1 day to permit the swelling of the GO film. The 2θ value of the as-prepared GO membrane was 9.76, which corresponds to the 9.1 Å interlayer spacing. When the GO film was immersed in an aqueous solution, the 2θ value decreased to 6.79, which corresponds to 13 Å because of the intercalation of water molecules in the GO sheet interlayers.

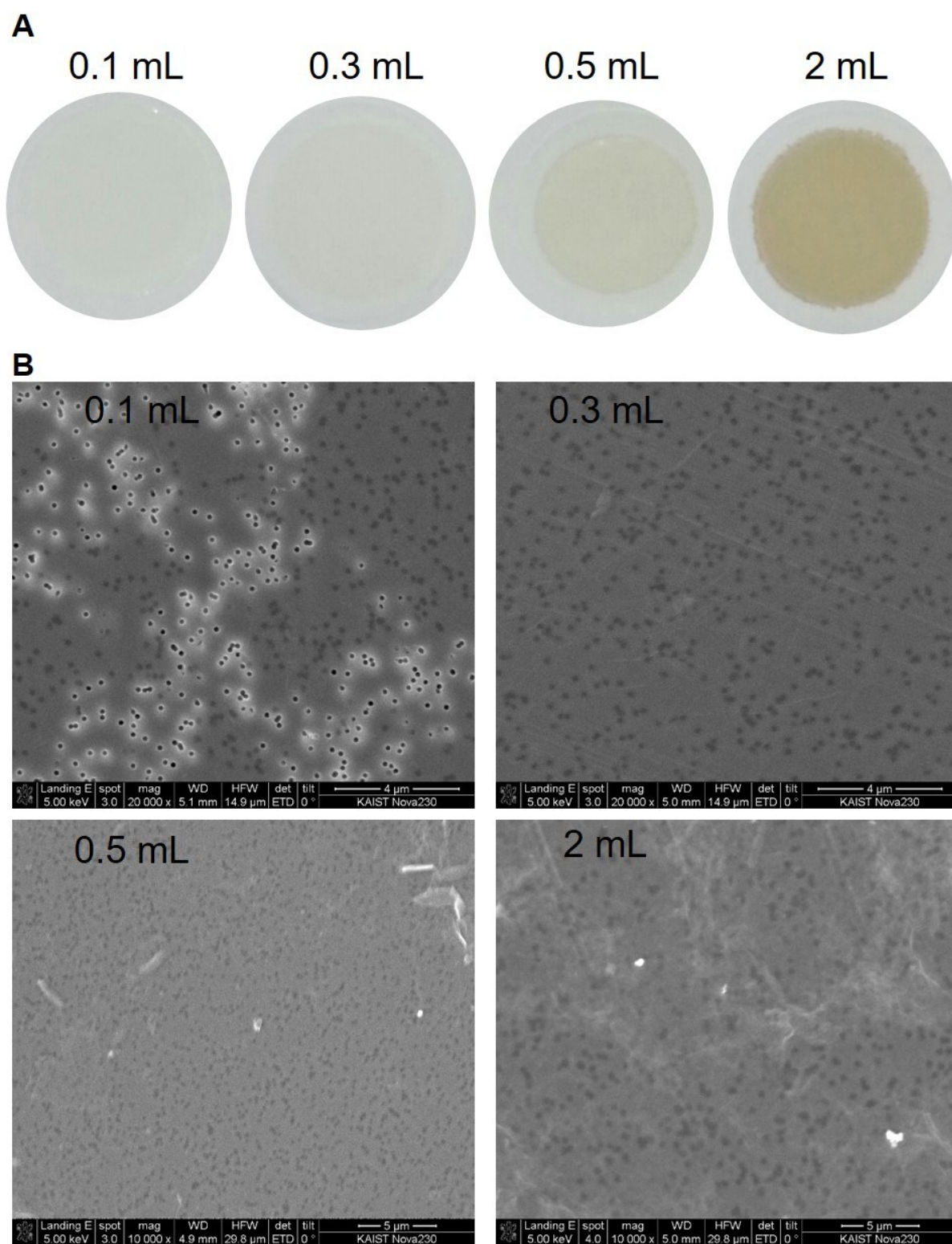


Fig. S13 Dependence of the coverage of the PC filter on the amount of the utilized GO solution (0.1 mg/mL). (A) Photographs and (B) SEM images of the GO/PC membrane with the varying amounts of the utilized GO solution. In our experiments, the GO membrane thickness linearly increased with the increase in the amount of GO for filtration from several nanometers to 40 nm. When the total amount of GO was 0.01 mg, the PC filter was not entirely covered with GO film; as full coverage was achieved with 0.03 mg of GO.

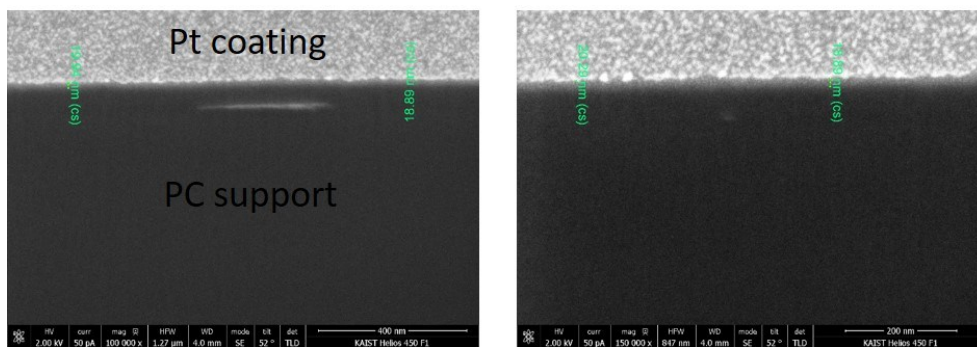


Fig. S14 Cross-sectional SEM images of the GO film (approximate thickness of 20 nm) after the filtration of 1 mL of a 0.1 mg/mL GO solution. In the case of 0.3 mL of the GO solution, the membrane was too thin to be observed by SEM.

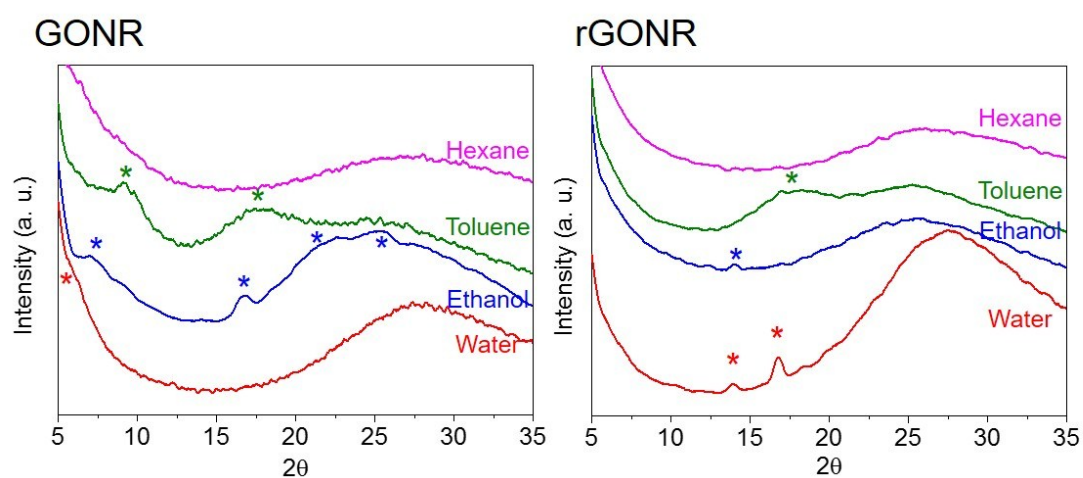
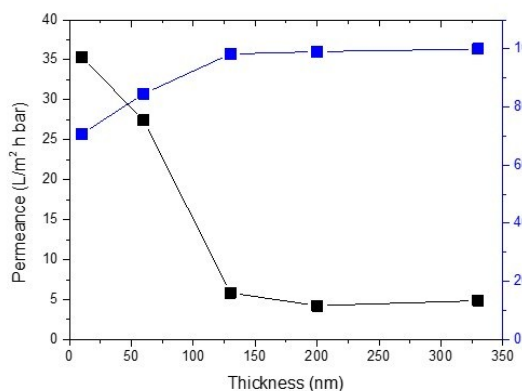


Fig. S15 XRD patterns of the GONR and rGONR membrane after swelling in water, ethanol, toluene, and hexane. Membranes were immersed in each solvent for 1 week to provide sufficient time for the intercalation of solvents into the membranes. Diffraction peaks are marked with *. For hexane, no particular diffraction peaks were observed possibly because of the sizes of interlayers, which were beyond the range of XRD observation.

GONR



rGONR

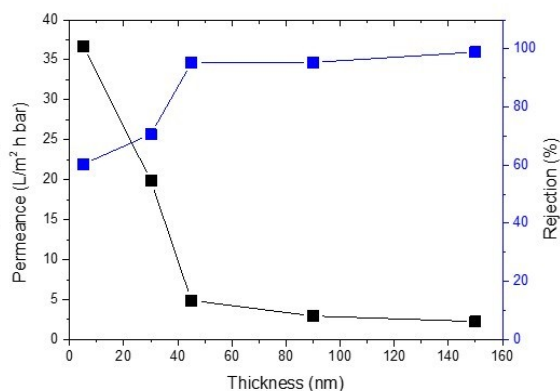
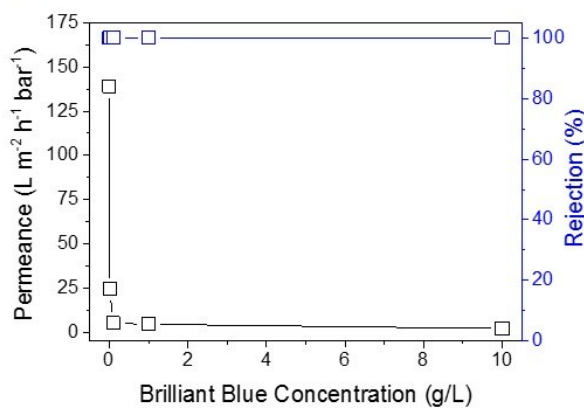
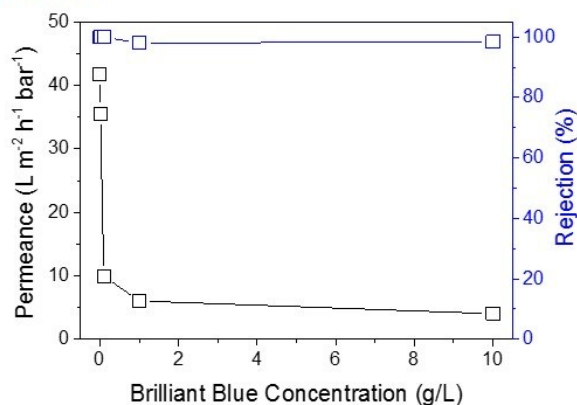


Fig. S16 Dependence of the performance of the GONR and rGONR membranes on the membrane thickness for the filtration of BB solution (10 mg/mL) at 5 bar.

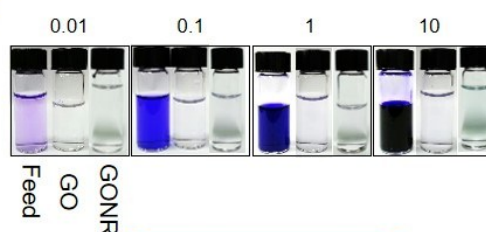
A GO



B GONR



C



D

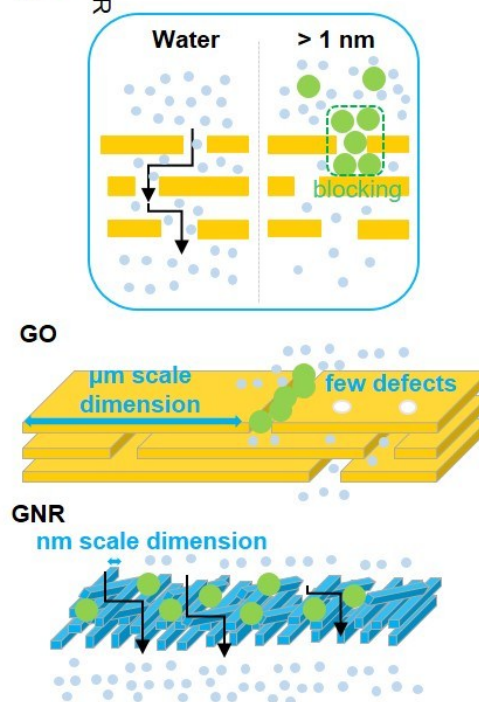


Fig. S17 Decline in water flux through 5 nm thick GO membrane and 100 nm thick GONR membrane. (A) and (B) Permeance and rejection rate for BB solutions increase with the concentration from 0.01 to 10 g/L. (C) Photographs of the solutions before and after filtration. (D) Schematics of the decline in water flux caused by the pore blockage of the GO and GONR membranes by the filtered molecules.

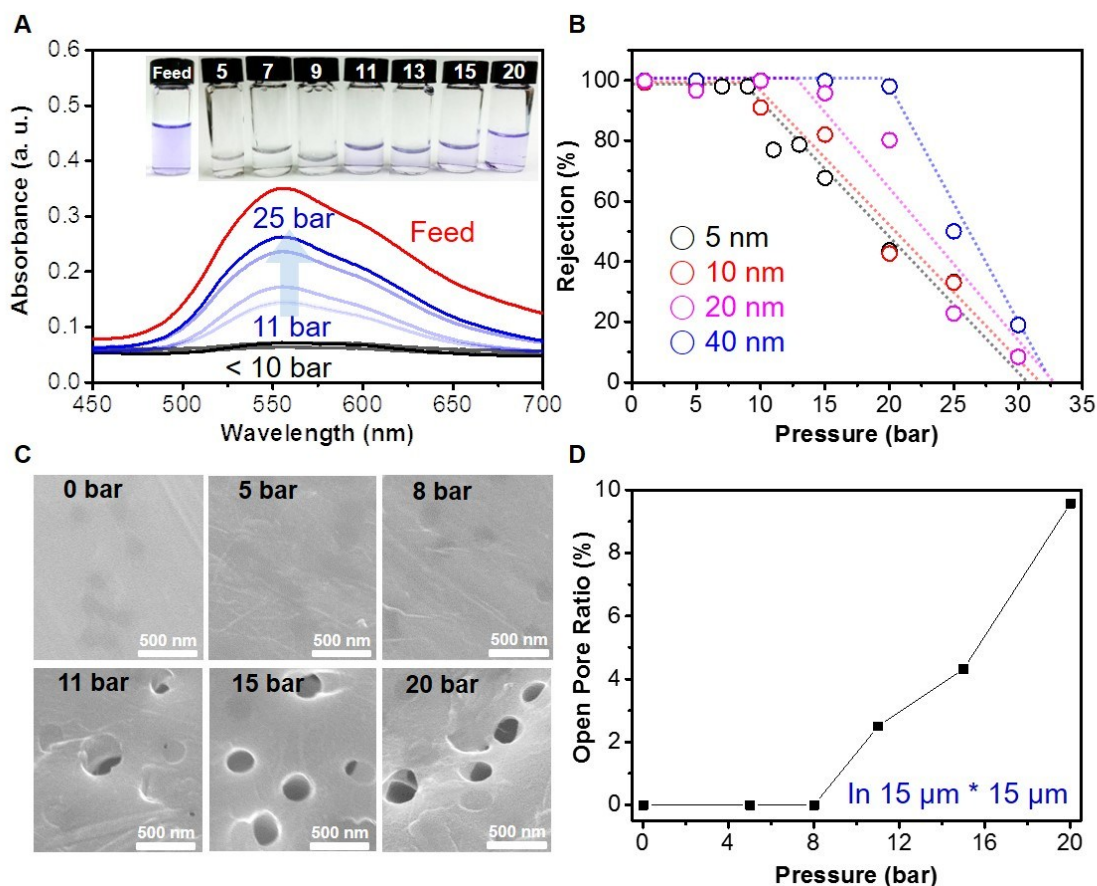


Fig. S18 Mechanical stability of the GO membrane. (A) UV-visible absorbance of the BB solutions filtered through 5 nm thick GO membrane. The concentration of the feed solution was 10 mg/L. Insets show photographs of the solution before and after filtration at various pressures. (B) Variation of rejection rates for the BB solutions with the GO film thickness and pressure. (C) SEM images of 5 nm thick GO membranes after filtration of BB solution as the pressure was increased from 0 to 20 bar. (D) Variation of the open-pore ratio of the GO membrane with the pressure applied on the PC supports.

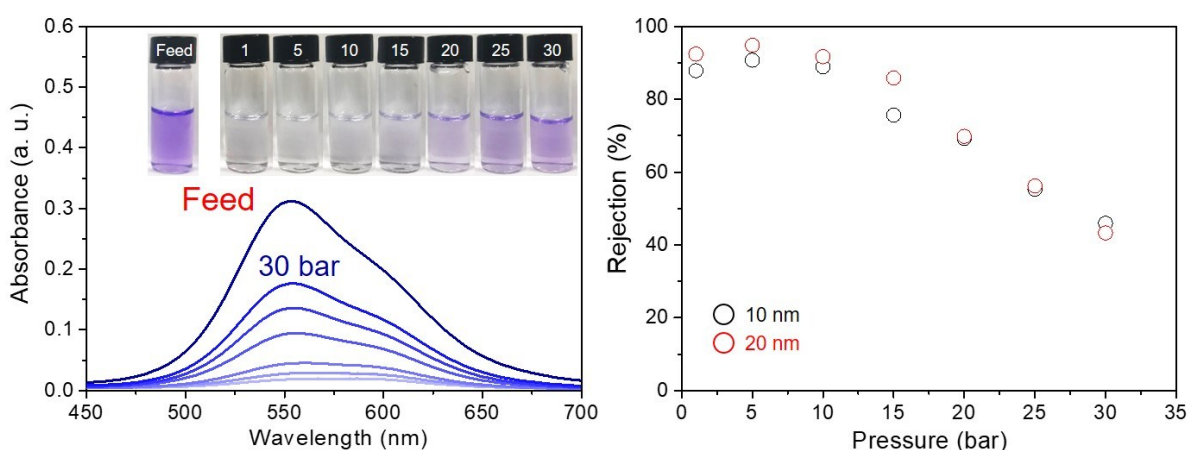
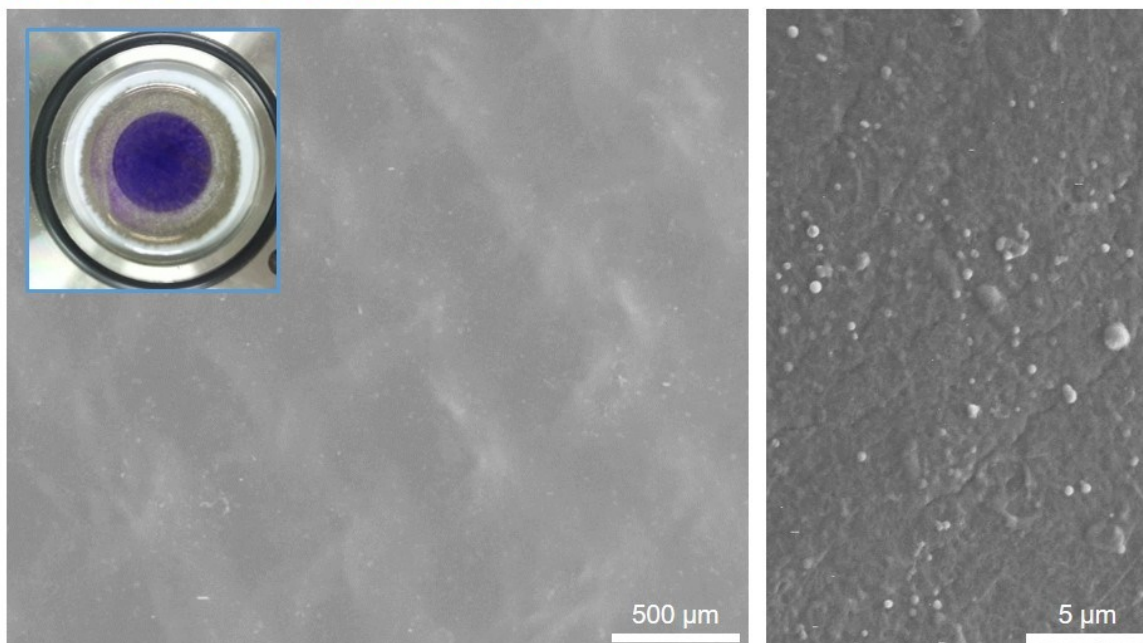


Fig. S19 Mechanical stability of RGO membrane. (A) UV-Visible absorbance of filtered Brilliant Blue solutions by RGO membrane with 20 nm thickness. Concentration of feeding solution was 10 mg/L. Insets are photographs of solution before and after filtration depending on the pressure. (B) Rejection of Brilliant Blue solutions depending on the RGO film thickness and pressure, respectively.

A 50 nm rGONR at 50 bar



B 300 nm rGONR at 50 bar

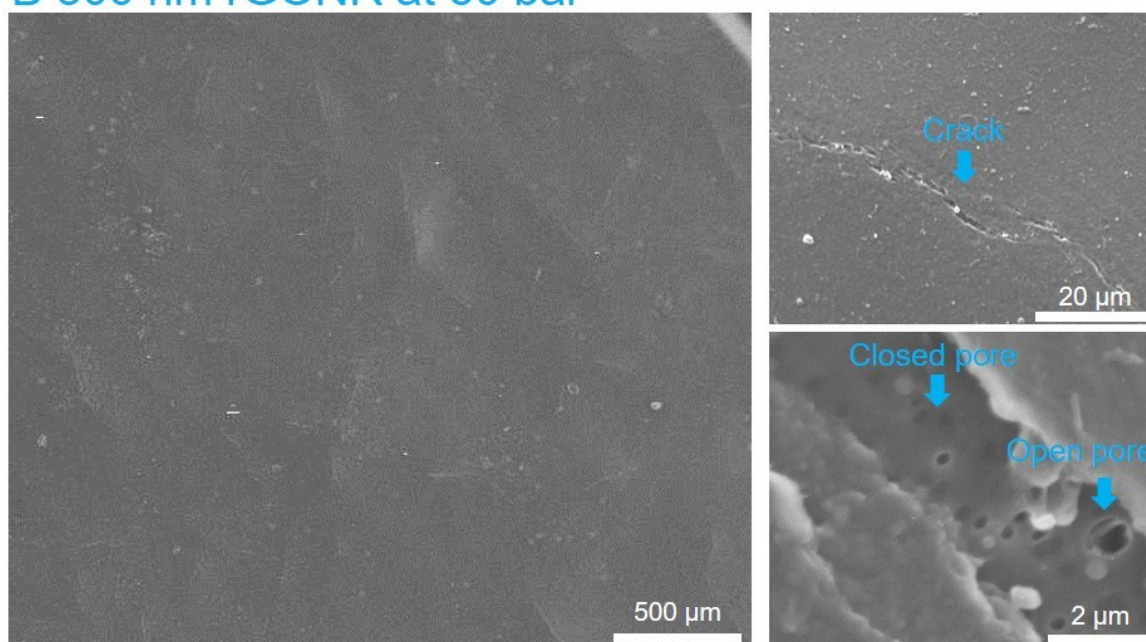


Fig. S20 SEM images of the (A) 50 nm thick and (B) 300 nm thick rGONR membranes after BB filtration at 50 bar. Inset is a photograph of the rGONR membrane after filtration. The polymer supports appeared to be stretched at high pressure (approximately 50 bar), following the shape (a check-like pattern) of the support of the membrane test equipment.

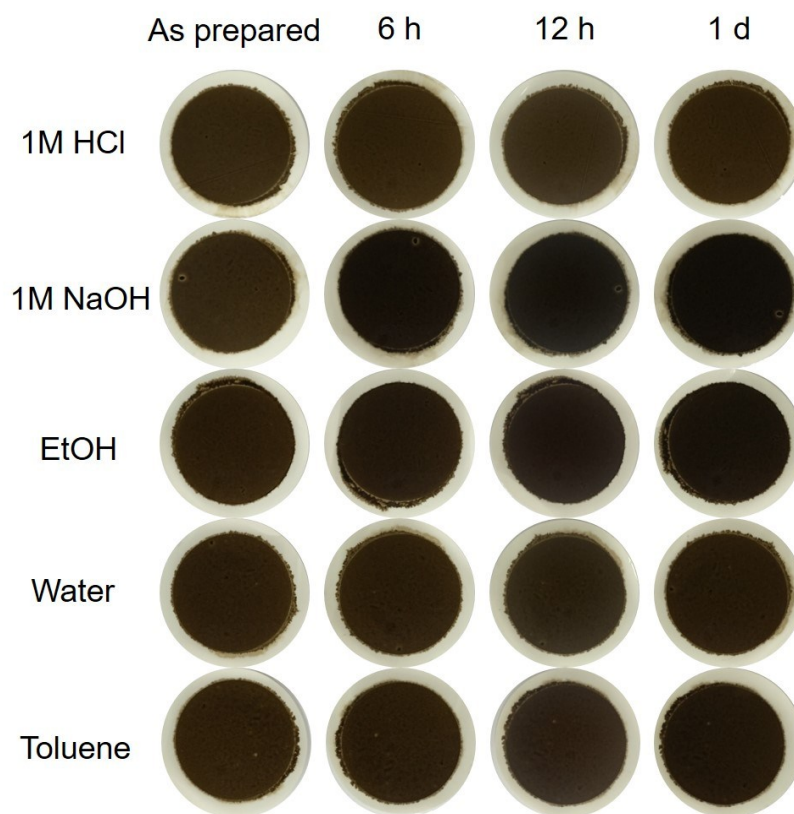


Fig. S21 Stability of the GONR membranes in various solvents. GONR membranes (~100 nm thickness) were immersed in 1 M HCl solution, 1 M NaOH solution, ethanol, water, and toluene for 1 day. No delamination of GONR films occurred during the immersion.

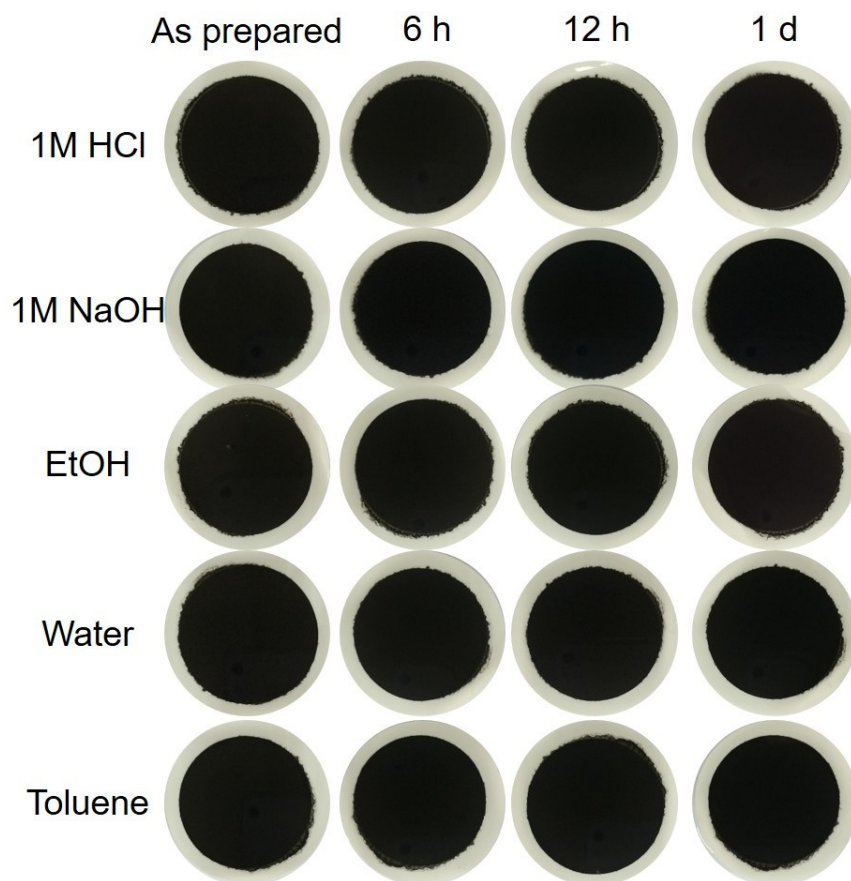


Fig. S22 Stability of the rGONR membranes in various solvents. rGONR membranes (~100 nm thickness) were immersed in 1 M HCl solution, 1 M NaOH solution, ethanol, water, and toluene for 1 day. No delamination of rGONR films occurred during immersion.

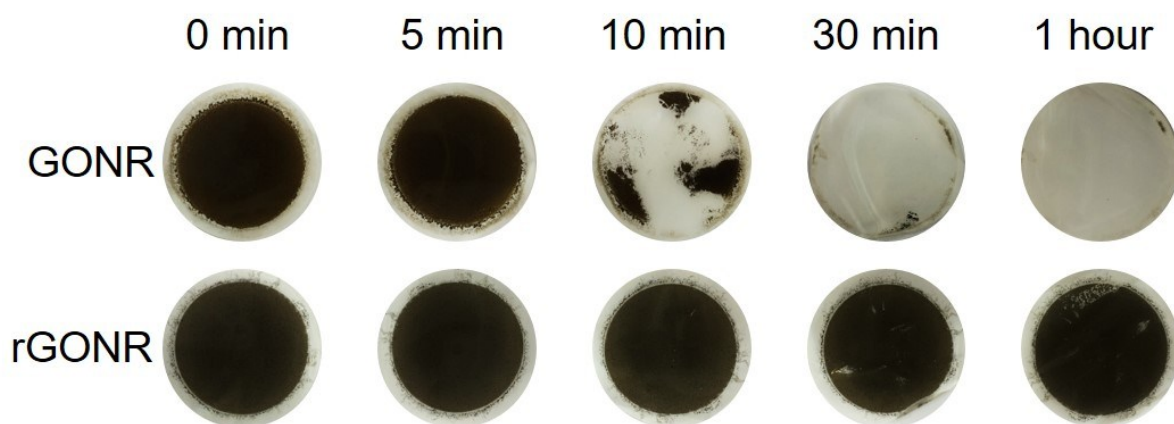


Fig. S23 Sonication of GONR and rGONR films in water. Because of the weak adhesion of GONR and rGONR films on the polymer support (PC), the films broke into small pieces and detached from the support rather than redispersing in the water during sonication. The rGONR membrane was highly stable under high-energy sonication (>1 h duration, 40 kHz frequency) in aqueous solution.

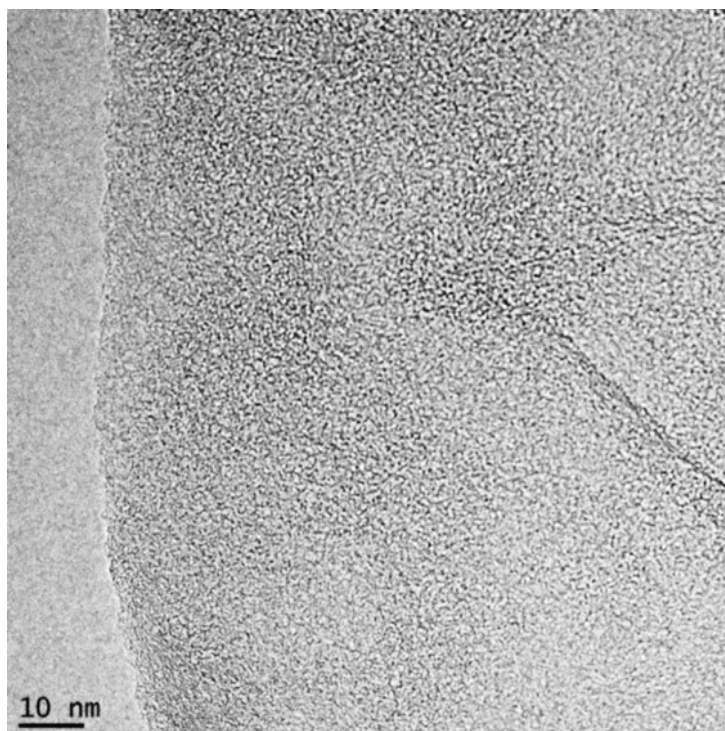


Fig. S24 TEM image of graphene oxide film, showing its uniform carbon layer.

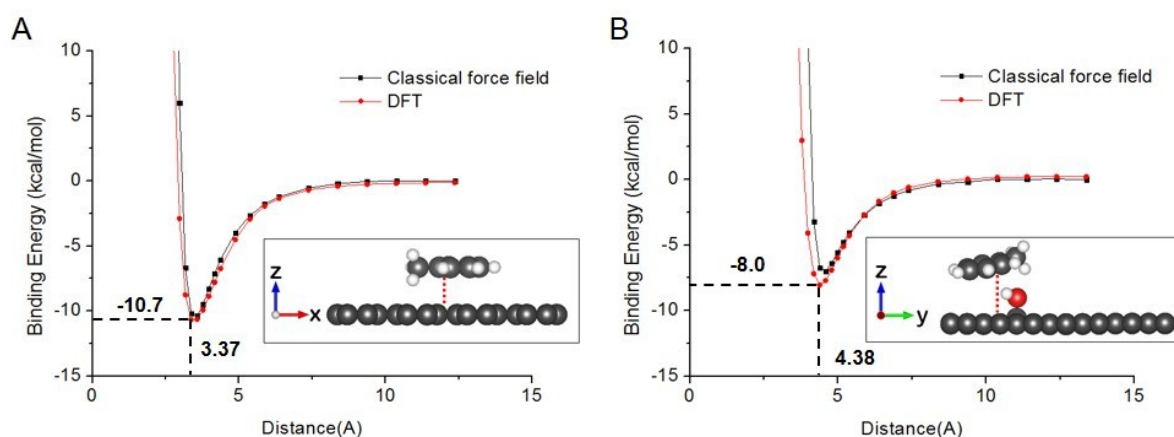


Fig. S25 Binding energy for toluene on (A) graphene and (B) GO as a function of the z distance between toluene and graphene. Force field calculations (black) were compared against DFT calculations (red).

To understand the effects of oxygen functional groups on the toluene flow relative to the flow on pristine graphitic channel, we performed DFT calculations to estimate the strength of binding of toluene to graphitic carbon *versus* that of binding to oxidized carbon. MD simulations were performed to compare the force-driven flow of toluene molecules between pristine graphitic channels *versus* that between oxidized graphitic channels. Hydroxyl groups, typical functional groups on graphene oxide, remain numerous in the long-term quasi-equilibrium state. [11] Therefore, we focused on hydroxyl groups of interlayer. As shown in **Fig. S25**, the binding of toluene to graphitic region (10.7 kcal/mol) was stronger than toluene–oxidized carbon interactions (8.0 kcal/mol) by 2.7 kcal/mol, and the energy minimum of the toluene–graphitic region interaction occurred at a distance (3.37 Å) shorter than that for the toluene–oxidized carbon interaction (4.38 Å). This difference may be explained by the favorable π – π bond interactions between toluene and pristine graphitic regions, which are weakened by the oxygen groups on the walls.

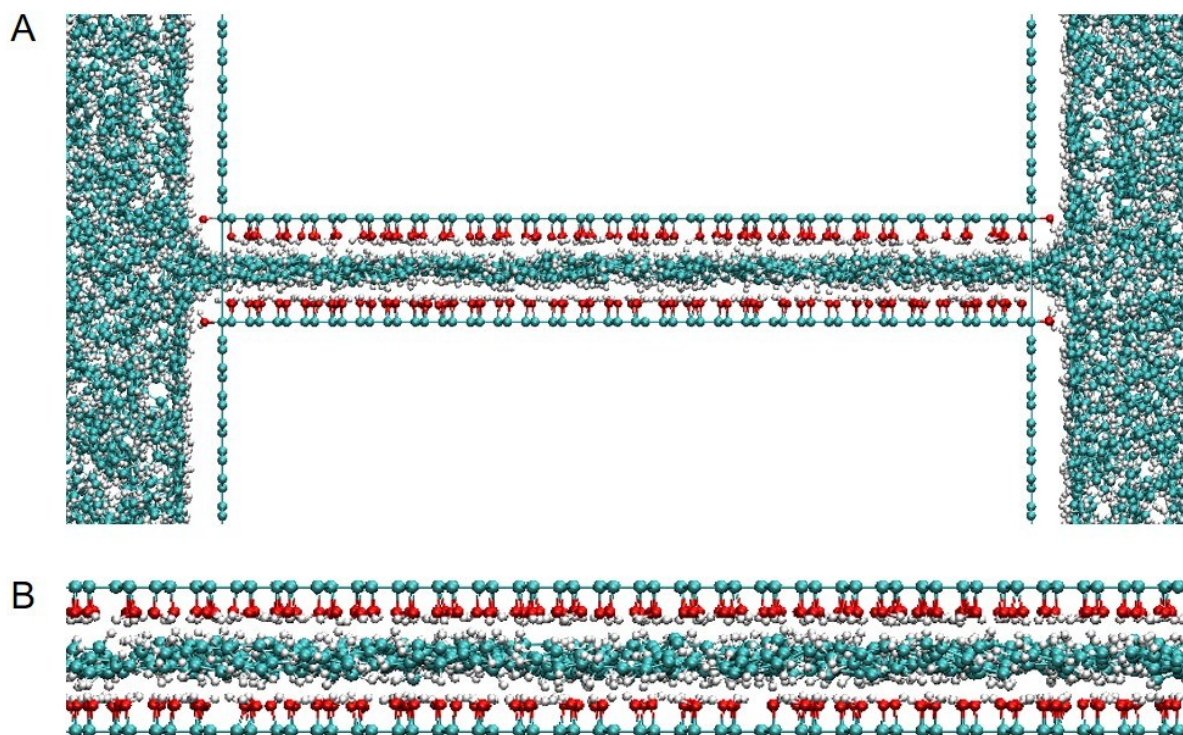


Fig. S26 Snapshots of the (A) reservoir model and (B) infinite-plate model used for MD simulations of toluene flow.

References

- [1] D. V. Kosynkin *et al.*, *Nature* 2009, **458**, 872.
- [2] R. R. Nair, H. A. Wu, P. N. Jayaram, I. V. Grigorieva and A. K. Geim, *Science* 2012, **335**, 442.
- [3] G. Kresse and J. Furthmüller, *Phys. Rev. B* 1996, **54**, 11169.
- [4] B. Hammer, L. B. Hansen and J. K. Nørskov, *Phys. Rev. B* 1999, **59**, 7413.
- [5] S. Grimme *et al.*, *J. Chem. Phys.* 2010, **132**, 154104.
- [6] S. Plimpton, P. Crozier and A. Thompson, *Sandia National Laboratories* 2017, **18**.
- [7] T. A. Pascal, K. Naoki and W. A. Goddard III, *J. Chem. Phys.* 2010, **133**, 134114.
- [8] S. L. Mayo, B. D. Olafson and W. A. Goddard, *J. Phys. Chem.* 1990, **94**, 8897.
- [9] R. Devanathan, D. Chase-Woods, Y. Shin and D. W. Gotthold, *Sci. Rep.* 2016, **6**, 29484.
- [10] W. L. Jorgensen, D. S. Maxwell and J. Tirado-Rives, *J. Am. Chem. Soc.* 1996, **118**, 11225.
- [11] S. Kim *et al.*, *Nat. Mater.* 2012, **11**, 544.